Journal of Statistical Physics, Vol. 77, Nos. 5/6, 1994

Brownian Dynamics of Polydisperse Colloidal Hard Spheres: Equilibrium Structures and Random Close Packings

W. Schaertl[1,2] and H. Sillescu[1]

Received January 25, 1994; final June 14, 1994

Recently we presented a new technique for numerical simulations of colloidal hard-sphere systems and showed its high efficiency. Here, we extend our calculations to the treatment of both 2- and 3-dimensional monodisperse and 3-dimensional polydisperse systems (with sampled finite Gaussian size distribution of particle radii), focusing on equilibrium pair distribution functions and structure factors as well as volume fractions of random close packing (RCP). The latter were determined using in principle the same technique as Woodcock or Stillinger had used. Results for the monodisperse 3-dimensional system show very good agreement compared to both pair distribution and structure factor predicted by the Percus–Yevick approximation for the fluid state (volume fractions up to 0.50). We were not able to find crystalline 3d systems at volume fractions 0.50–0.58 as shown by former simulations of Ree *et al.* or experiments of Pusey and van Megen, due to the fact that we used random start configurations and no constraints of particle positions as in the cell model of Hoover and Ree, and effects of the overall entropy of the system, responsible for the melting and freezing phase transitions, are neglected in our calculations. Nevertheless, we obtained reasonable results concerning concentration-dependent long-time self-diffusion coefficients (as shown before) and equilibrium structure of samples in the fluid state, and the determination of the volume fraction of random close packing (RCP, glassy state). As expected, polydispersity increases the respective volume fraction of RCP due to the decrease in free volume by the fraction of the smaller spheres which fill gaps between the larger particles.

KEY WORDS: Brownian dynamics simulations; colloidal hard spheres; polydispersity; random close packing.

[1] Institut für Physikalische Chemie, Johannes Gutenberg-Universität Mainz, 55099 Mainz, Germany.

[2] To whom correspondence should be addressed.

0022-4715/94/1200-1007$07.00/0

1. INTRODUCTION

Colloidal hard spheres provide an experimental system of major interest for many researchers. This is mainly caused by their analogy to simple atomic systems, with the important advantage of easy access to dynamics and structure of the magnified "quasiatomic" samples by common experimental techniques, such as, for example, dynamic light scattering,[1-5] video microscopy,[6-9] ultramicroscopy,[10-12] or SAXS.[13,14] Although modern techniques of polymer synthesis such as suspension, emulsion, and microemulsion polymerization[15-18] yield spherical colloidal particles in a size range of radius 10–1000 nm, the uniformity of these products is certainly not perfect as in true atomic systems. It is also not possible to prepare samples with adjusted definite polydispersities or to characterize the size and polydispersity of a colloidal system by analytical methods such as dynamic light scattering or electron microscopy without uncertainties. Since polydispersity truly influences the behavior of the sample compared to the ideal monodisperse system it usually is supposed to represent, it is necessary to find some way for detailed analysis of these effects on structure, dynamics, and phase behavior. As mentioned before, quantitative treatment of polydispersity effects by experiment is, due to the difficulties in preparation of very well-defined systems, nearly impossible, whereas this subject is, in most cases, by far too complicated for theoretical analytical solutions. Only numerical simulations seem to provide a technique which allows for investigation of all qualities of well-defined systems.

In the last 25 years, there have been many interesting developments concerning techniques for the numerical treatment of model systems, supported by a vast advance in computer technology. In principle, there exist three different approaches: the Monte Carlo method (MC),[19,20] the molecular dynamics technique (MD),[20-22] and the Brownian dynamics algorithm (BD), which is based on the position Langevin equation of colloidal suspensions derived by Ermak and McCammon.[23,24] Many investigations of charged colloidal systems based on MC[25,26] or BD[27-29] are found in the literature. Due to the nonanalytic form of the interaction pair potential of colloidal hard spheres, it is impossible to treat these systems in a numerically exact way using standard Brownian dynamics techniques. Recently, two different approaches to this problem have been published by Cichocki and Hinsen[30,31] and Schaertl and Sillescu.[32] We have shown elsewhere[32] that, while both algorithms yield the same results concerning particle dynamics in the extrapolated limit of infinitely short calculation time steps, which also correspond very well to theoretical[33] and experimental[3,9,34] predictions, our algorithm is more efficient considering convergence and equilibration, especially at very high particle

volume fractions $\phi > 0.50$. The details of this algorithm with accurate analysis of convergence as well as errors at finite calculation time steps are given in ref. 32. We have discussed the dynamics on different time scales and concentrations in monodisperse 2- and 3-dimensional hard-sphere suspensions and the effect of sample dimensionality, introducing a simple geometrical model to enable comparison of particle concentrations of samples with different dimensionality.

In this paper, we concentrate on the equilibrium pair distribution and structure factor of monodisperse 2- and 3-dimensional samples as well as 3-dimensional systems with Gaussian particle radius distribution. The structure factors are calculated by n-dimensional discrete Fourier transform of the sampled density profile which is calculated from the stored configuration data of the particles. Results of the 3-dimensional monodisperse systems are compared with theoretical predictions from the Percus–Yevick approximation[35–40] which should be valid for description of the structure of colloidal hard-sphere systems at not too high particle concentrations ($\phi < 0.40$). Crystallization should be found in the concentration regime $\phi = 0.50$ (freezing point) to $\phi = 0.54$ (melting point) as predicted by simulations from Hoover and Ree[41] and experiments from Pusey and van Megen.[42] However, no crystallization occurs in our simulations since the systems are not in thermodynamic equilibrium, i.e., the calculations started from random initial configurations and, at very high concentrations, structural relaxation might be too slow to reach the equilibrated state within the finite time of our calculations. The effect of different crystalline and random initial configurations upon the structure after long simulation times will be treated in a future publication. Here, it should be noted that the metastable glassy state which corresponds to a random close-packed (RCP) structure could not be obtained using a FCC initial configuration at $\phi \geqslant 0.60$. We will present a simple technique based on our BD algorithm and the principle of simulation of continuously growing spheres up to random close-packed conditions used in earlier work of Woodcock[43,44] and Lubachevsky and Stillinger[45] which enables us to determine the volume fraction of the RCP dependent on the polydispersity of the system. These results may be very important for interpretation of experimentally measured volume fractions at the glass transition compared with theoretically expected values. We will also present pair distribution functions and structure factors of polydisperse systems and give a brief discussion of the dependence of long-time self-diffusion coefficients on polydispersity and particle volume fractions.

2. BASIC CONCEPTS

2.1. Algorithm

Our computer algorithm for numerical treatment of colloidal hard-sphere suspensions has been presented in detail elsewhere.[32] Here, we just wish to give a brief summary of the principal idea:

We start our simulations of $N = 729$ particles with periodic boundary conditions and mean particle radius $R = 0.5\ \mu m$ from randomly chosen initial configurations and proceed as follows in each of the successive time steps τ (fixed to 0.5 msec for all simulations presented in this paper), calculating the time development of our system for a formal duration of 20 sec after 2 sec of equilibration:

1. Each particle is moved by the distance $(2D_0\tau)^{0.5}$ in one of the randomly chosen directions along each Cartesian axis ($\pm x$, $\pm y$, $\pm z$), where D_0 is the diffusion coefficient of the system without interactions as given by the Stokes–Einstein equation ($= 4.4 \times 10^{-13}\ m^2/sec$ in water at 20°C).

2. Any particle overlap detected after the move is corrected by pairwise shifting of the interfering particles up to their touching distance.

We store only 100 particle configurations with a time spacing of 0.2 sec. These data are used for later evaluation and calculation of physical properties such as time-dependent and long-time self-diffusion coefficients, pair distribution functions, or static structure factors.

The algorithm for determination of the RCP volume fraction is based on this simple technique: starting at a medium volume fraction of $\phi = 0.45$, steps 1 and 2 are repeated $N = 4000$ times until equilibration is reached, which corresponds to a time development of the system of $N\tau = 2$ sec. In the equilibrium state, the number of touching (or slightly overlapping!) particles is stored as a function of volume fraction. Before the next run, which starts from the preceding equilibrium configuration, each particle radius is increased by a factor of 1.005, which leads to an effective increase of the particle volume fraction by a factor of 1.015. This procedure is repeated until the number of touching (and overlapping) particles exceeds 723, and the corresponding final effective volume fraction is *defined* as the particle concentration of the RCP. Later, we will present a plot of the number of touching particles as a function of volume fraction for samples with radius polydispersity 20%. We will also discuss the dependence of ϕ_{RCP} on the standard deviation σ of the Gaussian polydispersity profile.

2.2. Gaussian Polydispersity Profile

The Gaussian polydispersity profile of particles with mean radius r_0 and standard deviation σ is given by

$$P(r) = C \exp[-(r - r_0)^2/2\sigma^2] \tag{1}$$

In our simulations, we treated particle ensembles with finite particle number of $N = 729$ and polydispersities σ/r_0 ranging from 0.01 to 0.40. To obtain comparable results, we sampled the polydispersity profile in the range $r_0 \pm 2\sigma$ with sample spacing 0.2σ, distributing the spheres on these sample cells according to their statistical weight. Since, due to cutoff effects, this profile does not represent the true Gaussian profile, we calculated the volume fractions for Gaussian profiles with the same σ in order to get a semiquantitative estimate of these effects. A simple approximation of the volume fraction of polydisperse samples for small σ was given by Pusey[46]:

$$\phi = \phi_0[1 + 3(\sigma/r_0)^2] \tag{2}$$

In Table I we present the volume fractions of systems with different Gaussian-shaped polydispersity profiles. Here A corresponds to the results given by Eq. (2), B represents a profile of >100,000 spheres sampled in the range $\pm 5\sigma$ with sampling resolution 0.02σ, C corresponds to >200,000 spheres sampled in the range $\pm 2\sigma$ with resolution 0.01σ, and D represents the profile of 729 spheres used in our simulations ($\pm 2\sigma$, $\Delta r = 0.2\sigma$). The results B–D were determined from numerical calculations.

At not too large polydispersities ($\sigma < 0.20r_0$) the results of Eq. (2) (A) correspond very well to the most realistic profile (B). Table I also shows very strong cutoff effects for polydispersity profiles C and D, especially at polydispersities exceeding 0.15, whereas the different sampling rate and particle number of ensembles C and D have no dramatic effect (even at very high polydispersities $\sigma = 0.40r_0$!). It is obvious that neglect of the intervals from 2σ to 5σ and from -5σ to -2σ in C and D leads to

Table I. Effects of Various Sampling of Gaussian Polydispersity Profiles on Respective Volume Fractions for the Example $\phi_0 = 0.64$[a]

σ/R	0.010	0.050	0.075	0.100	0.150	0.200	0.250	0.300	0.350	0.400
ϕ_A	0.640	0.645	0.652	0.659	0.683	0.717	0.760	0.813	0.875	0.947
ϕ_B	0.640	0.645	0.651	0.659	0.683	0.716	—	—	—	—
ϕ_C	0.640	0.644	0.648	0.655	0.673	0.699	—	0.773	—	0.877
ϕ_D	0.640	0.644	0.650	0.656	0.676	0.703	0.739	0.782	0.833	0.893

[a] ϕ_D corresponds to Gaussian-shaped profiles used in our simulations. See text for explanation of A–D.

diminished volume fractions, because the symmetric radius distribution of the Gaussian profile corresponds to an asymmetric volume distribution, thus shifting the mean value of ϕ. A symmetric cutoff of the radius distribution, which does not affect the mean radius of particles, thus affects the mean volume of particles and consequently leads to a distinct decrease of the respective volume fraction. We will keep in mind these findings when we discuss our results concerning polydispersity effects on the volume fraction of RCP, representing the glassy state, for samples with Gaussian size distribution.

We also should mention that, concerning our calculations without particle growth and polydispersities σ/r_0 up to 0.10, the formal volume fraction ϕ_0 (corresponding to monodisperse systems with identical box dimensions as for polydisperse systems, and particle radius equal to the mean radius, r_0) given in the plots and discussions below does not represent the true volume fraction of the polydisperse system, defined as $\phi_D = \sum V_i/V_{box}$, $i = 1,..., N$ (V_i is the volume of sphere i, V_{box} the volume of the simulation box, $N = 729$). This is due to the fact that, for practical reasons, we chose the box dimensions of all systems according to the monodisperse reference system. Thus, polydisperse samples with the same box size and mean particle radius as their corresponding monodisperse system have a volume fraction exceeding the monodisperse value due to the same reasons as discussed above. Nevertheless, this increase is less than 2% and does not affect the structural equilibrium properties, pair distribution $G_2(r)$ and static structure factor $S(q)$.

On the other hand, in the case of dynamics characterized by the concentration dependence of the long-time self-diffusion coefficient D_L, we use the true particle volume fractions ϕ_D for interpretation of the results. In the steady growth simulations used to determine the RCP concentration we also will use these true particle volume fractions of the polydisperse samples. It should be noted that the effect of remaining particle overlaps in the stored particle configurations and the resulting decrease of the effective volume fractions, taken into account in detail in our earlier publication,[32] this time is completely neglected. This reduction of ϕ strongly depends on concentration and is up to $\phi = 0.58$ below 2%, so it should not influence our numerical results concerning the concentration dependence of $S(q)$ and $G_2(r)$ in this regime. On the other hand, during the determination of ϕ_{RCP} by the steady growth algorithm, we are interested in the number of touching (and overlapping) spheres, which should hardly be affected by remaining particle overlaps and the corresponding reduction of the effective volume fraction. This can easily be imagined by the fact that the random packed structure of the spheres is not influenced by the particle overlaps, but, concerning single-particle dynamics, the particle overlaps (and corre-

sponding decreased effective particle radii) could be interpreted as a kind of slight compressibility of some of the "hard spheres," which certainly influences the mean particle mobility (D_L).

2.3. Numerical Determination of $G_2(r)$ and $S(q)$

The equilibrium structure of a given system can be characterized both by its pair distribution function $G_2(r)$ and its static structure factor $S(q)$, the latter being simply the Fourier transform. Whereas in experiment as well as theory it is by far easier to get the data in Fourier space, for example, by simple scattering experiments such as SAXS[13,14] or static light scattering, computer simulations provide direct access to $G_2(r)$ via the particle configuration data. Obtaining $S(q)$ from the small, finite system of our simulation is a quite deficient and complicated procedure, as we will show further below. An attempt to obtain $S(q)$ in a direct manner by discrete Fourier transformation (FFT)[47,48] of $G_2(r)$ failed since the statistical accuracy of the $G_2(r)$ data was insufficient (average over only 100 configurations) and there exist certain artifacts produced by the discrete FFT algorithm. Thus, we chose to calculate the n-dimensional structure factor by n-dimensional Fourier transformation ($n=2$ or 3) of the n-dimensional space density which has been determined from the stored particle configurations. Q-space-averaging of this n-dimensional structure factor and renormalization with respect to the height of the first maximum and the large-q limit yielded our normalized $S(q)$. Table II gives the resulting q range and q resolution at different particle volume fractions.

In the case of monodisperse 3D samples, we will compare our results of $G_2(r)$ and $S(q)$ with predictions from the Percus–Yevick equation.[35–40] Numerical PY solutions for $G_2(r)$ have been determined by Throop and Bearman,[38] using numerical evaluation of the exact solution of the PY equation for the radial distribution function of a classical hard-sphere fluid found by Wertheim.[37] These results are tabulated in ref. 38 for the regime $r/(2R)=1-3.95$ (R = hard-sphere radius) and volume fractions ranging from 0.052 to 0.576. We also have calculated $S(q)$ in the PY approxima-

Table II. q Range (from Zero to Maximum q Value q_m) and Resolution Δq of Calculated $S(q)$ for Different 3D Volume Fractions[a]

ϕ_0	0.10	0.20	0.30	0.40	0.50	0.60
q_m	2.05×10^4	2.58×10^4	2.95×10^4	3.25×10^4	3.50×10^4	3.72×10^4
Δq	640	806	923	1016	1094	1163

[a] q data in cm^{-1}.

tion, according to an analytical expression derived by van Beurten and Vrij.[49] Although PY approximations may yield invalid results at very high volume fractions ($\phi \geqslant 0.40$), nevertheless these deviations are within the uncertainty of our $G_2(r)$ data, which are comparably noisy, due to the statistical averaging over only 100 configurations. Thus we have chosen to compare our results, on a qualitative level, with the PY predictions. Due to the noisiness of our data we also omitted a quantitative comparison with the predicted contact values $G_2(r=2R)$. Concerning the polydisperse systems, unfortunately we have not been able to find appropriate theoretical predictions corresponding to the polydispersity distributions and very high concentrations ($\phi \geqslant 0.50$) treated in our simulations.

3. RESULTS

3.1. Equilibrium Structure of Monodisperse 3D and 2D Samples

Figures 1a and 1b present our results for $G_2(r)$ of monodisperse 3-dimensional hard-sphere systems at volume fractions $\phi = 0.366$ and 0.471 in comparison with theoretical PY predictions.[38] In both cases simulation data correspond very well to the theoretical predictions. So we can state that our simple (but effective) algorithm describes a realistic system of hard-sphere colloids with respect to hard-sphere interactions and their effects on equilibrium structure. It is remarkable that even for samples at higher concentrations the short equilibration period of 2 sec seems to be sufficient for the system to relax from randomly chosen particle positions to its equilibrium configurations. Nevertheless, one should bear in mind that our algorithm converges to a stationary state within finite evolution time, which is not necessarily the thermodynamic equilibrium, but may be metastable. Unlike Monte Carlo simulations searching for the minimum of free energy,[41] the shift procedure of our algorithm optimizes sphere packing with minimum overlap. Since no many-body correlations are considered, simulation runs may end up in random packing even for systems that should crystallize soon.

Figure 2 gives an example of $G_2(r)$ at higher concentration $\phi = 0.576$, where crystallization occurs in experiment[42] as well as in simulations which take into account thermodynamic properties of the system.[41] The second solid line with two peaks in the regime $r = 1.75$–$2.25\ \mu m$ corresponds to the simulation of a 2-dimensional sample with area fraction $\phi_A = 0.80$. At this concentration, the 2D sample shows a hexatic quasi-crystalline structure which has been proved by viewing the real-space configuration of the sample. Comparing the PY result at this concentration

with our 3D simulation data (small squares), we find distinct deviations. Our Brownian dynamics (BD) $G_2(r)$ shows two peaks at $r = 1.75$ and 2.0 μm, which seems to indicate some kind of hexagonal ordering for the 3-dimensional system at $\phi = 0.576$, corresponding perhaps to a disordered crystalline FCC phase as predicted in the literature.[41,42] Nevertheless, these small effects are still rather different from the expected $G_2(r)$ of the true FCC crystalline systems. Once again, we emphasize that our BD algorithm yields realistic equilibrium structures at volume fractions up to $\phi = 0.50$, where the PY approximation for colloidal hard-sphere systems still should be valid within the numerical accuracy of our $G_2(r)$, but it seems that it cannot be used for investigation of the crystalline phase behavior in the concentration regime $0.50 < \phi < 0.59$[42] if random initial

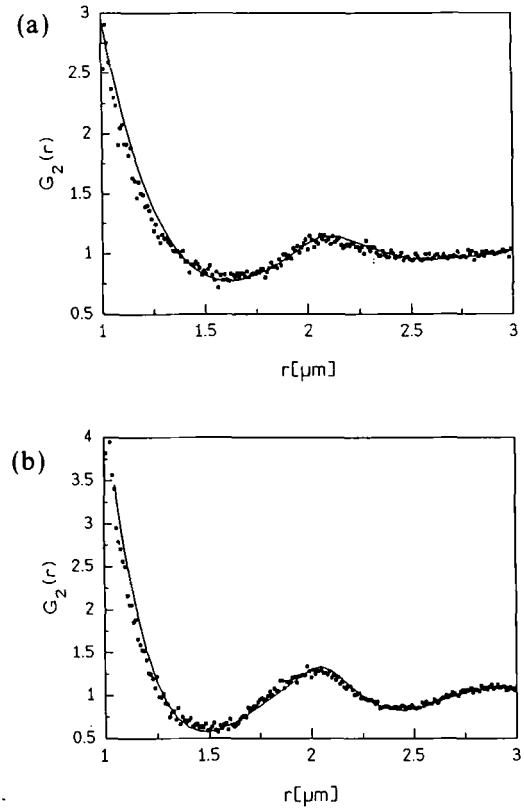

Fig. 1. (a) Comparison of $G_2(r)$ from numerical PY solutions[38] (line) with simulation results (symbols) for a monodisperse 3D System with $\phi = 0.366$, simulation $G_2(r)$ averaged over 100 configurations. (b) Same, with $\phi = 0.471$.

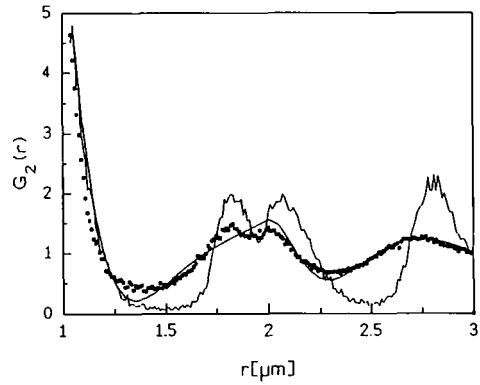

Fig. 2. $G_2(r)$ from PY[38] (smooth line) and 3D simulation (symbols) at $\phi = 0.576$. For comparison, $G_2(r)$ from simulation of a 2-dimensional system with $\phi_A = 0.80$ (jagged line with three maxima) is included.

configurations are used, at least not within the short evolution time of about 25 sec used so far. On the other hand, we should be able to investigate the glass transition of hard-sphere systems, which is expected in the regime $0.60 < \phi < 0.64$ and is based on the freezing in of translational motion in samples with RCP structure. This glassy state does not depend on thermodynamic properties, but should simply exist due to the geometrical constraints of the random close-packed structure. It should be noted that Woodcock, using a MD algorithm with steady particle growth,[43] also was not able to find crystallization of his samples, but could identify the glass transition of hard-sphere systems. Our investigations of the glassy state and its dependence on polydispersity of the sample will be presented further below.

In Figs. 3a and 3b results of $S(q)$ for monodisperse 3-dimensional samples at volume fractions 0.30 and 0.50 are presented in comparison with data calculated from an analytical PY equation.[49] As stated above, the equilibrium structure of our systems corresponds very well to the theoretical predictions at concentrations $\phi \leqslant 0.50$.

At the end of this section we present results concerning the structure of 2-dimensional monodisperse hard-sphere systems. We have already presented $G_2(r)$ at $\phi_A = 0.80$ (cf. Fig. 2). Figure 4 shows $S(q)$ of a highly crystalline hexatic structure at crystalline close packing ($\phi_A = 0.90$). In this case crystallization is simply caused by geometrical constraints and less dependent upon higher-order correlations, which are neglected in our calculations. At this point, let us emphasize that of course our systems are

thermodynamically stable in the sense of having constant temperature (which was shown from the behavior of short-time diffusion[32]) and exhibiting no convection flux.

3.2. Equilibrium Structure of Polydisperse 3D Samples

Figures 5a and 5b show plots of $G_2(r)$ at volume fractions $\phi_0 = 0.50$ and $\phi_0 = 0.60$ for monodisperse systems and systems with polydispersity $\sigma/r_0 = 0.10$. Whereas the amorphous state ($\phi_0 = 0.50$) exhibits no sizable differences between monodisperse and polydisperse systems, $G_2(r)$ shows strong deviations at $\phi_0 = 0.60$. For $\sigma/r_0 = 0$, we find two peaks at $r = 1.7$–2.1 μm, which may indicate the strongly disordered FCC structure

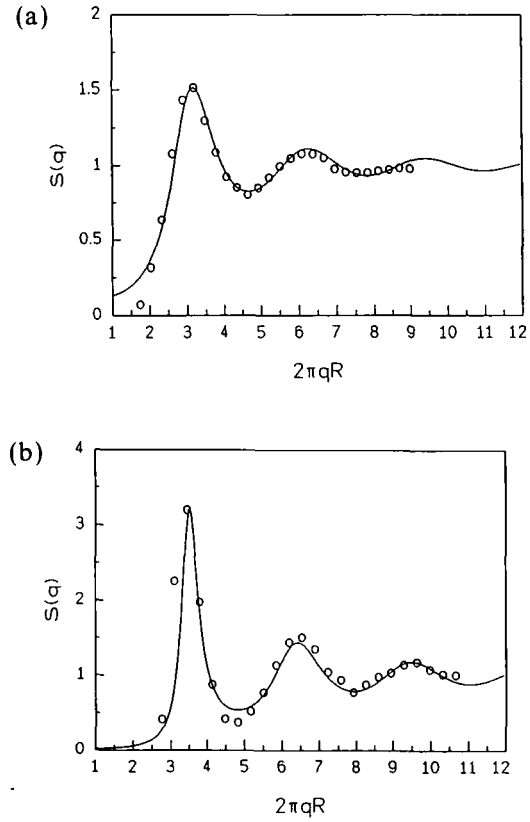

Fig. 3. Renormalized $S(q)$ from simulation (circles) and calculated $S(q)$ [see ref. 49] (line) for a monodisperse 3D sample with (a) $\phi = 0.30$ and (b) $\phi = 0.50$.

mentioned already for $\phi_0 = 0.576$ (Fig. 2). This double peak structure is not seen in the polydisperse system. Furthermore, the amplitudes of the oscillations of $G_2(r)$ are diminished, meaning that the spatial regime of the shell of next neighbors is less defined than in the monodisperse system. There also is a shift of the first maximum toward smaller values of r, which corresponds to the possibility of smaller next-neighbor distances caused by the fraction of smaller particles in our polydisperse sample.

Next, let us consider the results for $S(q)$ given in Figs. 6a and 6b. For practical reasons nonrenormalized $S(q)$ are used. Note that, due to the insufficient q resolution, we are not able to detect a significant shift of the first maximum in either case. At $\phi = 0.50$ a polydispersity of $\sigma/r_0 = 0.05$ has only slight effects on the first and second maxima of $S(q)$, and $\sigma/r_0 \geqslant 0.10$ is needed to obtain significant deviations. In the system with higher concentration, $\phi_0 = 0.60$, polydispersities as small as $\sigma/r_0 = 0.05$ lead to similar deviations in $S(q)$ as for $\sigma/r_0 = 0.10$ in the former. In general, larger polydispersities result in reduction of the peak amplitudes of $S(q)$, which corresponds to a less developed structure and definition of the spatial nearest-neighbor regime as stated above. These reasonable results correspond to common theoretical[50,51] and experimental[52] findings. In the literature, a polydispersity of $\sigma/r_0 \geqslant 0.06$ is supposed to be sufficient to inhibit crystallization of hard-sphere systems.[53,54]

In Table III we show the effect of polydispersity on reduced long-time self-diffusion coefficients D_L/D_0 as calculated according to[32]

$$D_L = \langle r^2(\Delta t)\rangle/(6\,\Delta t), \qquad \Delta t = 5 \text{ sec} \tag{3}$$

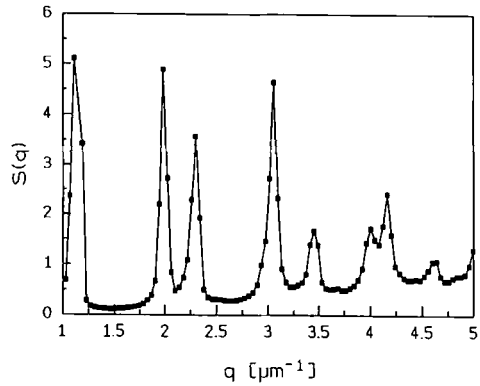

Fig. 4. $S(q)$ determined from simulation of a monodisperse 2-dimensional system at crystalline close packing ($\phi_A = 0.90$).

In all cases, D_0 was chosen according to the monodisperse reference system, because in the case of small radius polydispersities below 10% this value corresponds very closely to the Stokes–Einstein diffusion coefficient averaged over all particles of the polydisperse ensemble. Correspondingly, in every case the mean squared displacements used in Eq. (3) were determined from averaging over all particles, whereas concerning the Brownian motion of each particle, its actual radius is used for calculation of the Stokes–Einstein diffusion coefficient, which governs its random displacement during the elementary calculation step. Although there seems to be a small deviation in D_L/D_0 with increasing polydispersity at larger volume fractions, this is only due to the increase of particle volume fractions in the

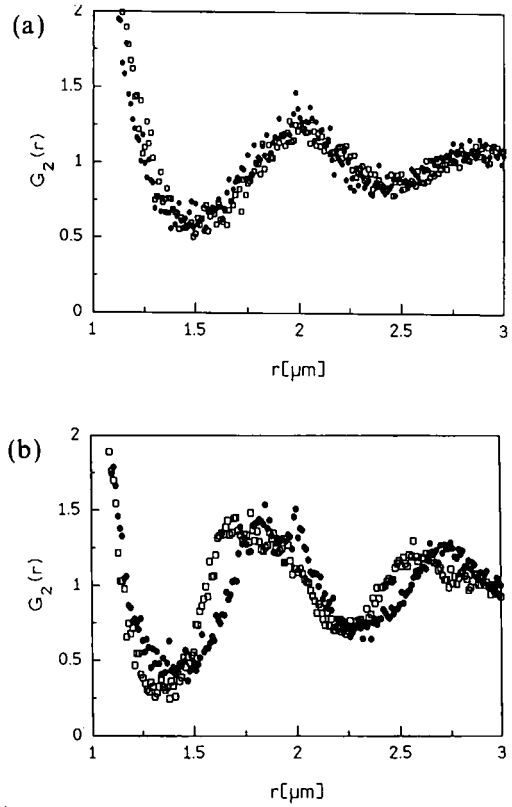

Fig. 5. $G_2(r)$ from simulations of a 3-dimensional monodisperse (filled symbols) and a polydisperse system, $\sigma/r_0 = 0.10$ (open symbols) at formal (see text) volume fraction (a) $\phi_0 = 0.50$ and (b) $\phi_0 = 0.60$.

polydisperse system (see Table I, row D). For comparison, Table IV gives the true volume fractions ϕ_D of our systems with Gaussian-shaped polydispersity.

It should be noted, as stated above, that the box dimensions of our simulated systems were chosen according to the monodisperse systems with volume fractions ϕ_0. In the polydisperse systems the same box size and mean particle radius are used, which leads to an effectively increased volume fraction (see above). The data given in Table III show that small radius polydispersities below 10% ($\sigma/r_0 = 0.10$) have no effect on long-time particle mobility (D_L) at volume fractions $\phi_0 < 0.60$. In the case of

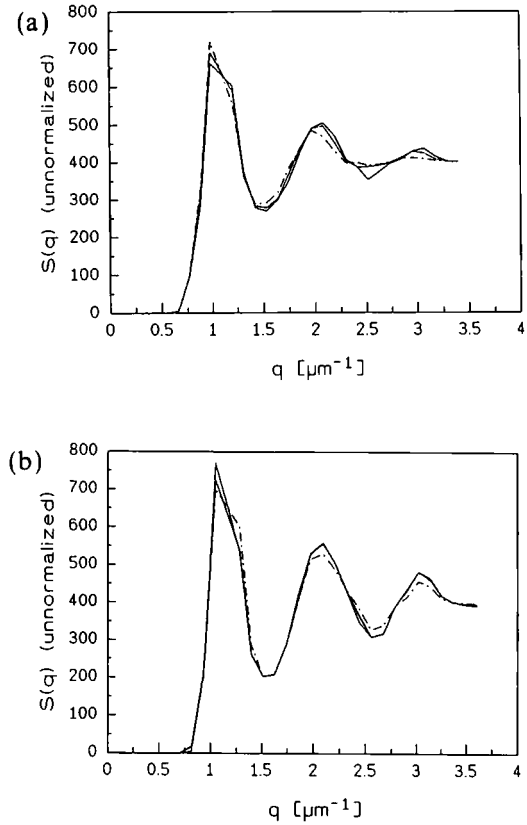

Fig. 6. (a) $S(q)$ (unnormalized, see text) from simulations of 3-dimensional systems with polydispersities $\sigma/r_0 = 0.00$ (solid line), 0.05 (dotted line), and 0.10 (dash-dotted line) and formal $\phi_0 = 0.50$. (b) $S(q)$ from 3D systems with $\sigma/r_0 = 0.00$ (solid line), 0.01 (dotted line), and 0.05 (dash-dotted line) and formal $\phi_0 = 0.60$.

Table III. Reduced Long-Time Self-Diffusion Coefficients of Polydisperse Systems[a]

ϕ_0	0.10	0.20	0.30	0.40	0.50	0.60
$D_L(\sigma=0.00)/D_0$	0.83	0.67	0.50	0.34	0.16	0.015
$D_L(\sigma=0.02)/D_0$	0.83	0.67	0.50	0.34	0.16	0.014
$D_L(\sigma=0.06)/D_0$	0.84	0.67	0.50	0.34	0.16	0.010
$D_L(\sigma=0.10)/D_0$	0.84	0.68	0.49	0.33	0.15	0.009

[a] $D_0 = 4.4 \times 10^{-13}\ m^2\ sec^{-1}$.

$\phi_0 = 0.60$, there is a decrease of D_L from samples with $\sigma/r_0 = 0.00$ to $\sigma/r_0 = 0.06$ which is caused by the increase of the true volume fractions ϕ_D with increasing polydispersity σ (see Table IV). On the other hand, no decrease in particle mobility is found comparing $\sigma/r_0 = 0.06$ and 0.10, although the true volume fraction of the system with higher polydispersity is significantly larger. This can be understood from the fact that the smaller particles of our Gaussian size distribution need less free volume for single-particle motion than the particles of a comparable monodisperse system because of their smaller hard-sphere radius. Thus, the long-time self-diffusion coefficient of polydisperse systems, which is calculated as an average value over all spheres of the polydisperse ensemble, using D_0 according to the monodisperse reference system, is larger than that of a monodisperse sample with equal true volume fraction ϕ_D. In general, samples with higher degrees of polydispersity have larger volume fractions of close packing due to the possibility of smaller particles to "fill the gaps" between the larger ones. These effects of polydispersity on the random close-packed structure will be discussed in more detail in the next section.

3.3. Determination of Φ_{RCP} of Polydisperse Systems

We used the steady growth algorithm in association with our technique of numerical treatment of colloidal hard-sphere interactions, described

Table IV. Increase of True Volume Fraction Φ_D Depending on Polydispersity σ[a]

$\phi_0 =$	0.100	0.200	0.300	0.400	0.500	0.600
$\sigma = 0.02$	0.100	0.200	0.300	0.400	0.500	0.601
$\sigma = 0.06$	0.101	0.202	0.303	0.404	0.504	0.605
$\sigma = 0.10$	0.102	0.205	0.307	0.410	0.512	0.615

[a] Given are various ϕ_0 and corresponding ϕ_D (cf. Table I).

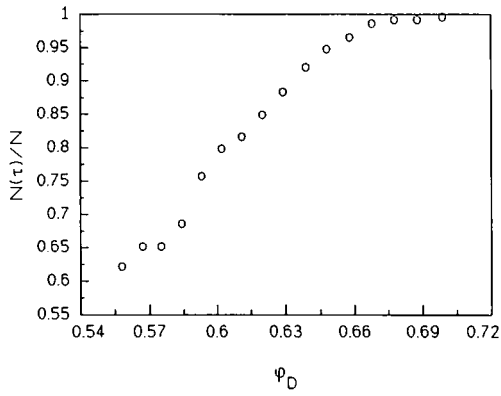

Fig. 7. Concentration dependence of the fraction of touching spheres, $N(\tau)/N$, for systems with polydispersity $\sigma/r_0 = 0.20$.

above, to determine the volume fraction of random close packing of samples with various degrees of polydispersity ranging from $\sigma/r_0 = 0.00$ to 0.40. Figure 7 shows the concentration dependence of the number of touching spheres for a system with $\sigma/r_0 = 0.20$. At high concentrations, the asymptotic approach to 100% overlapping particles is very slow; thus it is difficult to determine the volume fraction of RCP without uncertainties. We have defined as ϕ_{RCP} the volume fraction where no more increase was found in the number of touching particles $N(\tau)$. At this concentration, $N(\tau)$ was always larger than 723, giving a close-packed state of 99.2% of the sample, which seems to be sufficient within numerical error. The corresponding uncertainty of ϕ_{RCP} is estimated to be of the order of about ± 0.01. Table V gives a summary of our results of ϕ_{RCP} for various values of σ/r_0.

As expected, we find a strong increase of ϕ_{RCP} with increasing σ, caused by the filling of the gaps of the smaller fraction of particles, which reduces the free volume. This effect should be considered for interpretation of experimental data on the glass transition of nonuniform samples. Effects of polydispersity seem to be negligible, within experimental uncertainties of 5%, for samples with σ/r_0 up to 0.05. Since many systems in experimental

Table V. Random Close Packing of Polydisperse Samples

σ	0.00	0.02	0.05	0.075	0.10	0.15	0.20	0.25	0.30	0.35	0.40
ϕ_{RCP}	0.64	0.65	0.66	0.66	0.67	0.68	0.68	0.69	0.71	0.74	0.78

practice have larger polydispersities, our calculations may provide some useful hints concerning data analysis of results that appear unexpected from the point of view of monodisperse samples.

4. CONCLUSIONS

We have shown that our new algorithm for the treatment of hard-sphere interactions in Brownian dynamics simulations[9,32] provides also efficient ways to find the equilibrium structure for volume fractions $\phi < 0.50$ as was shown by comparison of $G_2(r)$ and $S(q)$ with the Percus–Yevick approximation (Figs. 1 and 3). In the crystalline phase transition regime, $0.50 < \phi < 0.54$, our algorithm yields partial hexagonal or FCC ordering (Fig. 2) when starting from random initial particle positions within finite evolution time (the effect of different initial configurations upon the resulting structure and dynamics will be treated elsewhere[55]). We have also simulated polydisperse systems using a discrete approximation to a Gaussian distribution of sphere radius. In the fluid state ($\phi_0 < 0.50$), the influence of polydispersity upon $G_2(r)$ and $S(q)$ is almost negligible for $\sigma/r_0 \leqslant 0.10$. At $\phi_0 \geqslant 0.5$, the partial hexagonal ordering seen in monodisperse samples is blurred and becomes undetectable for $\sigma/r_0 = 0.10$ (Fig. 5). The volume fractions at random close packing, ϕ_{RCP}, are found to increase with increasing polydispersity as expected. The average long-time self-diffusion coefficient D_L is relatively independent of σ if normalized to D_0 and ϕ_0 of the corresponding monodisperse system, since the decrease due to large ϕ_D (see Table I) is balanced by the increase due to the higher mobility of a system "lubricated" by the small spheres of the size distribution.

ACKNOWLEDGMENT

Support by the Fonds der Chemischen Industrie is gratefully acknowledged.

REFERENCES

1. M. M. Kops-Werkhoven and H. M. Fijnaut, *J. Chem. Phys.* **77**:2242 (1982).
2. A. van Veluven, H. N. W. Lekkerkerker, C. G. de Kruif, and A. Vrij, *J. Chem. Phys.* **89**:2810 (1988).
3. W. van Megen and S. M. Underwood, *J. Chem. Phys.* **91**:552 (1989).
4. V. Degorgio, R. Piazza, M. Corti, and J. Stavans, *J. Chem. Soc. Faraday Trans.* **87**:431 (1991).

5. E. Bartsch, M. Antonietti, W. Schupp, and H. Sillescu, *J. Chem. Phys.* **97**:3950 (1992).
6. C. A. Murray and D. H. van Winkle, *Phys. Rev. Lett.* **58**:1200 (1987).
7. W. Schaertl, Ph.D. thesis, Mainz University (1992).
8. A. Kasper, Diploma thesis, Mainz University (1993).
9. W. Schaertl and H. Sillescu, *J. Colloid Interface Sci.* **155**:313 (1993).
10. A. Kose, M. Ozaki, K. Takano, Y. Kobayashi, and S. Hachisu, *J. Colloid Interface Sci.* **44**:330 (1973).
11. R. Williams and R. S. Crandall, *Phys. Lett. A* **48**:225 (1974).
12. H. Yoshida, K. Ito, and N. Ise, *J. Am. Chem. Soc.* **112**:592 (1990).
13. S. Stoelken, Ph.D. thesis, Mainz University, in preparation.
14. E. B. Sirota, H. D. Ou-Yang, S. U. Sinka, P. M. Chaikin, J. D. Axe and Y. Fujii, *Phys. Rev. Lett.* **62**:1524 (1989).
15. E. B. Bradford and J. W. Vanderhoff, *J. Appl. Phys.* **26**:864 (1955).
16. J. W. Vanderhoff, *Prepr. Am. Chem. Soc. Div. Org. Coat. Plast.* **24**:223 (1964).
17. M. Antonietti, W. Bremser, D. Müschenborn, Ch. Rosenauer, B. Schupp, and M. Schmidt, *Macromolecules* **24**:6636 (1991).
18. V. Frenz, Ph.D. thesis, Mainz University, in preparation.
19. K. Binder, *Monte Carlo Methods in Statistical Physics* (Springer, 1986).
20. H. Gould and J. Tobochnik, *An Introduction to Computer Simulation Methods*, Parts 1 and 2 (Addison-Wesley, 1988).
21. B. J. Alder and T. E. Wainwright, *J. Chem. Phys.* **31**:459 (1960).
22. L. Verlet, *Phys. Rev.* **159**:98 (1967).
23. D. L. Ermak, *J. Chem. Phys.* **62**:4189/4197 (1975).
24. D. L. Ermak and J. A. McCammon, *J. Chem. Phys.* **69**:1352 (1978).
25. M. O. Robbins, K. Kremer, and G. S. Grest, *J. Chem. Phys.* **88**:3286 (1988).
26. N. Pistoor and K. Kremer, *Prog. Colloid Polymer Sci.* **81**:184 (1990).
27. H. Löwen and G. Szamel, to be published (1993); H. Löwen, private communication.
28. R. Klein, W. Hess, and G. Nägele, *Physics of Complex and Supramolecular Fluids* (Wiley, New York, 1987).
29. I. Snook and W. van Megen, *J. Colloid Interface Sci.* **100**:194 (1984).
30. B. Cichocki and K. Hinsen, *Physica A* **166**:473 (1990).
31. B. Cichocki and K. Hinsen, *Physica A* **187**:133 (1992).
32. W. Schaert and H. Sillescu, *J. Stat. Phys.* **74**:687 (1994).
33. M. Medina-Noyola, *Phys. Rev. Lett.* **60**:2705 (1988).
34. S. Möller, Ph.D. thesis, Mainz University, in preparation.
35. J. K. Percus and G. L. Yevick, *Phys. Rev.* **110**:1 (1958).
36. E. Thiele, *J. Chem. Phys.* **39**:474 (1963).
37. M. S. Wertheim, *Phys. Lett.* **10**:E501 (1963).
38. G. Throop and R. J. Bearman, *J. Chem. Phys.* **42**:2408 (1965).
39. W. R. Smith and D. Henderson, *Mol. Phys.* **19**:411 (1970).
40. D. Henderson and E. W. Grundke, *J. Chem. Phys.* **63**:601 (1975).
41. W. G. Hoover and F. H. Ree, *J. Chem. Phys.* **49**:3609 (1968).
42. P. N. Pusey and W. van Megen, *Nature* **320**:340 (1986).
43. L. V. Woodcock, *J. Chem. Soc. Faraday II* **72**:1667 (1976).
44. L. V. Woodcock, *Ann. N. Y. Acad. Sci.* **37**:274 (1981).
45. B. D. Lubachevsky, F. H. Stillinger, and E. N. Pinson, *J. Stat. Phys.* **64**:501 (1991).
46. P. N. Pusey, In *Light Scattering in Liquids and Macromolecular Solutions* (Plenum Press, New York, 1980).
47. W. K. Pratt, *Digital Image Processing* (Wiley, 1978).
48. R. W. Ramirez, *The FFT* (Tektronix, New Jersey, 1985).

49. P. van Beurten and A. Vrij, *J. Chem. Phys.* **74**:2744 (1981).
50. J. L. Lebowitz, *Phys. Rev.* **133**:A895 (1964).
51. A. Vrij, *J. Chem. Phys.* **69**:1742 (1978).
52. C. G. de Kruif, W. J. Briels, R. P. May, and A. Vrij, *Langmuir* **4**:668 (1988).
53. J. L. Barrat and J. P. Hansen, *J. Phys.* (Paris) **47**:1547 (1986).
54. P. N. Pusey, *J. Phys.* (Paris) **48**:709 (1987).
55. W. Schaertl and H. Sillescu, to be published.